Research Square

Preprints are preliminary reports that have not undergone peer review.
They should not be considered conclusive, used to inform clinical practice,
or referenced by the media as validated information.

Class A GPCR structures usually capture the kinetically preferred G protein without a universal geometric signature

Hossein Batebi

hbat@zedat.fu-berlin.de

Freie Universität Berlin https://orcid.org/0000-0002-0714-9700

Article

Keywords:

Posted Date: November 10th, 2026

DOI: https://doi.org/10.21203/rs.3.rs-11640484/v1

License: This work is licensed under a Creative Commons Attribution 4.0 International License.
Read Full License

Additional Declarations: There is **NO** Competing Interest.

Class A GPCR structures usually capture the kinetically preferred G protein without a universal geometric signature

Hossein Batebi

Department of Physics, Freie Universität Berlin, 14195 Berlin, Germany
hossein.batebi@fu-berlin.de | ORCID 0000-0002-0714-9700

Abstract

Cryo-electron microscopy reveals how G protein-coupled receptors (GPCRs) engage their G proteins, and AI-based prediction now models many more such complexes. But does the captured partner indicate which signalling route a receptor prefers? Here I compare 207 curated receptor–G protein structural units from 164 class A receptors with published G-protein activation data. In 81% of the 94 units with kinetic data, the captured family was also the most rapidly activated. Structural scores, however, predicted activation of uncaptured families only modestly, and this did not replicate in independent assays. Receptor geometry recognised the captured family beyond close homologues (AUC 0.73 versus 0.59 for conserved sequence positions at 50% identity), but class-wide differences such as TM6 opening largely vanished within the same receptor. A stable complex therefore shows which partner a receptor can accommodate, not necessarily which it prefers. Resolving preference will require time-resolved kinetic experiments and simulations of the steps preceding complex formation.

Introduction

G protein-coupled receptors (GPCRs) connect the outside of a cell to its internal signalling machinery. A single receptor can engage several G-protein families, each capable of initiating a different cellular response. Which partner it activates, and how quickly, can shape the outcome of the same chemical signal. Understanding this choice is central to pharmacology, including efforts to develop ligands that favour particular pathways[1–5]. Yet the G protein seen next to a receptor in a structural model is not a direct readout of that choice. To signal, the proteins must meet, rearrange and exchange nucleotides before they separate. A stable complex shows that an interaction can be accommodated under the conditions in which it was captured; it does not measure the likelihood or speed of productive activation.

Cryo-electron microscopy has now revealed many GPCR–G protein complexes in molecular detail, while AI-based structure prediction has greatly expanded the structures available for asking mechanistic questions[6–8]. The resulting models show the shape of the receptor's intracellular cavity and the contacts made by the G protein, and they have helped identify important features of coupling[9–20]. But most deposited complexes are stabilised, often nucleotide-free endpoints. They do not show every intermediate on the route from initial encounter to G-protein activation. Time-resolved studies of selected receptors have begun to capture parts of that process[20–24]. The question is therefore not whether these structures are informative, but how far their information extends to functional preference.

Previous studies have mapped functional coupling preferences, identified sequence and interface determinants, and shown that changing selected contacts can shift which G proteins a receptor activates[9,10,13–15]. These advances establish that molecular interactions contribute to selectivity; they do not tell us how reliably the geometry of a mature, experimentally captured complex reveals a receptor’s preferences among competing signalling routes. This matters because the structural archive is not a balanced survey of all possible couplings. Particular receptors, G proteins, ligands and stabilising conditions are selected for experimental tractability, while closely related receptors share much of their sequence and shape. A class-associated geometric pattern may therefore distinguish the complexes researchers have solved without representing a shared movement that controls partner choice within each receptor[18–20]. To determine what structural signatures actually tell us about function, they must be compared with independent activation measurements, tested against uncaptured signalling routes and examined both across divergent receptors and within the same receptor, with explicit safeguards against evolutionary relatedness[25].

To test this boundary, I combined a curated survey of experimentally determined class A GPCR complexes with published measurements of G-protein activation. Each analysed observation represents a receptor and the transducer family captured in a structural complex, not an independent experimental specimen or a claim about the receptor's preferred signalling route. I first ask whether the captured partner corresponds to the family's measured activation. I then examine whether receptor geometry recognises that partner more reliably than a defined sequence representation when closely related receptors are withheld. Finally, I compare structures of the same receptor with different G proteins,

including a limited set captured with different ligands. This approach identifies what can be inferred from mature complexes, while leaving the kinetics and molecular origins of partner selection to experiments that can observe them directly.

Results

Structural capture tracks prominent signalling routes imperfectly

I began with experimentally determined class A GPCR structures deposited in the Protein Data Bank, using GPCRdb and GproteinDb to standardise receptor and G-protein identities[26,27]. The survey included 1,360 structures. After removing repeated representations of the same receptor–transducer pairing and applying the predefined quality rules, the analysis comprised 207 structural units from 169 receptor entries, corresponding to 164 distinct receptors; 34 receptors had been solved with more than one G-protein class (Fig. 1). A structural unit here means a curated receptor paired with the family of G protein or family-representative transducer present in its deposited complex. It is not the same as a separately prepared specimen, and the captured family is not a measurement of functional preference. To avoid confusing the receptor's own shape with coordinates supplied by its partner, all geometry used for prediction was measured on the receptor alone. I also checked the experimental provenance of supposedly partner-free structures, since receptor-only coordinates can originate from focused refinement of particles that originally contained a transducer (Supplementary Fig. 9).

The first biological test was straightforward: when a receptor has been structurally resolved with a particular G protein, is that also the family it activates most rapidly? I compared captured partners against published onset measurements from a broad receptor panel[14]. Experimental rates overlapped with 94 structural units representing 77 receptors. I kept three outcomes distinct: the family present in a structure, the fastest family in the kinetic assay and whether any activation was detected. In particular, a recorded zero indicates activity below that assay's threshold, not proof that coupling is impossible. I also examined Gαq and Gα15 separately rather than silently treating their responses as interchangeable.

The correspondence was substantial, but incomplete. In 81% of the overlapping structural units, the captured family was also the fastest activated family in the kinetic panel (95% confidence interval, 73–89%; Fig. 2a). The kinetically preferred family was represented among captured partners for all but one receptor. This suggests that structural studies often sample prominent signalling routes, without establishing why those routes were preferentially captured. The clearest mismatch involved Gs: six receptors had a Gs-containing structure but no detectable Gs activation in the kinetic assay, despite measurable Gi/o or Gq/11 activation in that same panel. Four of those six showed evidence of Gs coupling in at least one other functional platform, however, including shedding or ebBRET measurements. The discrepancy therefore depends partly on the assay and its conditions. Engineered G-protein constructs, stabilising binders and experimental choices can further favour the capture of a complex that is not the most rapidly activated route in an unmodified cell.

I next asked whether structural information could reveal activity beyond the family already present in the complex. Using receptor-coordinate predictions made without functional-annotation inputs, I evaluated detectable activation of the two G-protein families not captured in each structure. The scores showed modest discrimination in the original kinetic panel (family-mean area under the receiver-operating-characteristic curve, AUC = 0.705; 95% receptor-clustered confidence interval, 0.586–0.827; Fig. 2b; Source Data 25). This association exceeded the conditional permutation control (P = 0.0005; Source Data 26), but depended on the biological definition of a positive response: counting Gα15 alongside Gαq lowered the AUC to 0.620 (Source Data 27). Only six positive cases contributed to the uncaptured-Gs component, making that estimate uncertain. Graded correspondence between structural scores and measured rates also failed to improve convincingly on the simple rule of ranking the already-captured family first (Supplementary Tables 36 and 40). Thus, recognition of a captured partner should not be mistaken for a general prediction of unobserved coupling or activation kinetics.

Independent functional datasets provided a more demanding check. Responses measured by ebBRET and receptor-mediated shedding did not reproduce the discrimination seen for the kinetic detection endpoint (AUC 0.500 and 0.542, respectively; Supplementary Table 39; Source Data 26). Importantly, those datasets include unreported responses that cannot be treated as confirmed negatives. Sequence was also a meaningful comparator: among receptors with matched functional labels, a simple sequence-

neighbour predictor trained using measured responses performed at least as well as the structural scores under ordinary receptor-held-out testing, while the differences under stricter homology separation were uncertain (Fig. 2c; Source Data 27). Because the neighbour method used measured kinetic labels and the geometry method was trained on structural classes, the comparison does not isolate the independent contribution of coordinates. Functional prediction from the mature endpoint is therefore context-dependent rather than a transferable selectivity rule. Independent live-cell biosensor studies likewise show that GPCR coupling profiles can depend on cellular context[28].

Receptor geometry recognises partners across distant receptors

Why, then, do mature structures contain a recognisable G-protein signature? To separate the question of structural recognition from functional preference, I compared two ways of predicting the family present in a deposited complex: selected amino acids in the receptor sequence and measurements of the receptor's intracellular geometry. Both predictors used receptor information only, not atoms from the bound G protein. I withheld entire receptors during evaluation and, more stringently, withheld groups of receptors with similar sequences. This design asks whether a structural pattern learned from one receptor can identify the captured partner of another, rather than merely recalling the close relatives represented in the training set.

With individual receptors withheld, sequence and geometry performed similarly on the captured-partner task (macro AUC 0.803 and 0.776, respectively; Fig. 3a). Their behaviour diverged when close homologues were excluded. At 50% sequence-identity separation, the independently refitted geometry model retained an AUC of 0.726, whereas the tested sequence encoding fell to 0.586. The paired geometry advantage remained positive when entire sequence-identity clusters were resampled (95% interval, +0.038 to +0.200; Source Data 28). A positive difference also appeared at 40% identity, although that comparison contained far fewer independent lineages and its magnitude depended on how models were tuned within the cross-validation folds (Supplementary Tables 34 and 45). These results show that receptor geometry can carry information about the partner captured by a mature complex beyond what the selected sequence positions captured in this benchmark. They do not imply that geometry is intrinsically superior to the full receptor sequence or to sequence models trained for other purposes.

Adding the selected sequence positions to the geometric descriptors did not improve discrimination under the strict identity-controlled comparisons (Fig. 3a). Nor could acquisition metadata alone account for the geometric signal: the acquisition-only model was near chance at 50% identity (Supplementary Table 33). The comparison therefore supports a real association between receptor shape and captured partner, while leaving open which molecular features, experimental conditions or receptor histories produced it. Learning-curve sensitivity is shown in Supplementary Fig. 3.

That association did not transfer indefinitely across the receptor family. Discrimination declined as the test receptors became more evolutionarily distant, and at the most stringent 30% sequence-identity split neither approach performed reliably. This should not be read as a biological cutoff: the archive then formed only five sequence clusters, one of which contained nearly all structural units, leaving just two usable and highly unequal test folds (Supplementary Fig. 11). Even at 40% identity, one large cluster dominated the held-out data. The better-supported observation is therefore transfer beyond close homologues at the 50% threshold, with a more tentative extension to 40%, not an exact evolutionary boundary. Interface sequence and evolutionary-transfer controls are shown in Supplementary Figs. 4 and 5.

Several checks strengthened this narrower interpretation. Removing functional-annotation variables from the original structural representation, and then excluding acquisition and selected completeness indicators, left the transfer pattern broadly intact (Supplementary Tables 33 and 34). Cluster-level resampling and analyses omitting the largest cluster from fixed held-out predictions continued to favour geometry at the 50% and 40% thresholds (Source Data 28). These checks address the possibility that a few related receptor groups or metadata fields created the result. They do not eliminate all selection bias, and the largest-cluster exclusions were not new model refits. The descriptive localisation and instability of sequence coefficients are shown in Supplementary Fig. 6.

A further question is whether the apparent class signature reflects a change induced by the bound partner or simply the fact that different receptors dominate different structural groups. Among the 34 receptors resolved with more than one G-protein class, a coordinate-only classification signal was small under receptor-held-out evaluation and weakened further as related receptors were excluded (Fig. 3c;

Supplementary Table 33). At 50% identity, the class-probability margin remained only slightly above the permutation control (+0.012, P = 0.011), and within-receptor accuracy was not distinguishable from it (50.0%, P = 0.26; Supplementary Table 33). This does not rule out meaningful local rearrangements, but it cautions against attributing the stronger across-receptor classification result to a universal change within each receptor.

Functional preference also follows receptor ancestry, though not in a way that defines a simple universal rule. Mapping published activation profiles onto a tree built from conserved receptor positions showed a significant phylogenetic association for the three G-protein families, and close homologues frequently shared their preferred partner (Supplementary Fig. 10). For more divergent receptor pairs, agreement approached that expected from the overall prevalence of each family. The measured preferences thus have an evolutionary structure, but the available sample cannot establish where that structure ceases or whether the limits of functional and structural transfer arise from the same molecular cause.

Two final checks clarify the scope of these findings. Simple measurements of receptor geometry identified structures annotated as active or inactive with very high accuracy, even across distant receptors (Supplementary Fig. 7). That positive control demonstrates recovery of a comparatively conserved structural state, not independent biochemical validation, because the annotations themselves come from structural studies. In contrast, structural capture cannot be read as exclusive coupling: more than half of the units linked to an external coupling map belonged to receptors with support for multiple G-protein families (Supplementary Fig. 8c). No tested cavity measurement independently tracked the number of detected families after adjustment for captured class. Predicting those additional couplings from the deposited structure was also weak: across 190 units from 156 receptors, endpoint geometry did not exceed chance under receptor-held-out testing (family-mean AUC 0.55, 95% CI 0.49–0.61), whereas full sequence reached 0.63 and a global sequence-identity baseline 0.66 (Fig. 4d). A receptor conformation can therefore carry a recognisable structural-state signature while leaving an important functional question unresolved.

Class-wide signatures weaken within individual receptors

The next test examined the geometry directly. If one shared molecular movement distinguishes Gs from Gi/o or Gq/11, that movement should be visible when the same receptor has been captured with different partners. Across the full archive, Gs-containing complexes do show a more open intracellular region, including a larger outward displacement of the sixth transmembrane helix (TM6) and changes around the TM6–TM7 cavity and the second intracellular loop (Fig. 4a; Supplementary Fig. 1). These differences are real associations in the deposited structures. The key question is whether they remain when receptor identity is controlled.

Most of the shared effect diminished in that comparison. For Gs versus Gi/o, the standardised difference in TM6 displacement fell from about three-quarters of a standard deviation across the archive to approximately one-tenth within receptors solved with both partners, with the within-receptor confidence interval spanning zero (Fig. 4b,c). Across the multi-partner subset, none of the measured intracellular descriptors survived correction for multiple testing. Nor did the direction of receptor deformation caused by the bound complex reveal a common class-specific movement beyond the permutation control. This does not mean that individual receptors lack structurally encoded selectivity; rather, many apparent class-wide differences reflect which receptors were included in each structural group, not a universal motion shared by them all. The full feature-by-class-pair screen is documented in Supplementary Fig. 2.

The G-protein side of the interface offered an independent place to look. I aligned structures of the same receptor captured with different G proteins and examined the position and orientation of the Gα α5 helix, which inserts into the receptor's intracellular cavity. This yielded 41 pairwise comparisons from 32 receptors. By holding the receptor reference frame fixed, the analysis asked whether different G-protein families use a common direction of movement at the mature interface, without assuming that α5 alone contains every determinant of selectivity.

The answer was again receptor-dependent. The aligned receptor cores and α5 positions generally differed only modestly, and the α5 displacement vectors showed no reproducible direction shared across receptors (Fig. 5a,b). Gi/o and Gs complexes differed more in α5 helix angle than the other class pairs, as expected from their established modes of engagement (Fig. 5c), but that difference did not amount to

one universal class-specific displacement. Comparisons involving Gs were also not stabiliser-matched, whereas the more numerous Gi/o–Gq/11 pairs shared scFv16. These constraints limit how strongly the negative result can be interpreted: an absence of a shared α5 shift in the observed endpoints does not exclude selective contacts or distinct intermediates during activation.

Different ligands can share related mature interfaces

Finally, a small within-receptor case series asked whether differences at the ligand-binding pocket must remain equally apparent at the mature G-protein interface. Five published cryo-EM structures of the serotonin 5-HT_1A receptor bound to Gi_1 were captured with chemically distinct ligands[29]. To account for differences between deposited Gα constructs, I compared ligand and receptor–Gα contact sets only within four pairs that shared the same annotated Gα construct category. In those descriptive comparisons, receptor contacts to Gα were more similar between structures than contacts to the ligands themselves, and the ordering persisted across the tested distance cutoffs (Supplementary Fig. 12; Source Data 29). However, these comparisons share structures and cannot be treated as independent experiments. Only three ligands had verified comparable quantitative Gi_1 maximal-response values, which spanned a narrow range; a separate four-receptor analysis did not reveal a uniform pattern. The case therefore illustrates that distinguishable ligand contacts can coexist with related mature interfaces. It neither establishes the determinants of ligand efficacy nor generalises to all GPCRs.

Discussion

Cryo-EM and structural prediction have changed what can be seen of GPCR signalling. In a mature complex, they identify how the receptor accommodates its partner, which regions make contact and which conformations are compatible with a captured molecular assembly. Those are substantial biological insights. They are not, however, the same as a measurement of how a receptor chooses among several potential partners. This study shows why that distinction matters: geometry can recognise the G protein present in a structure across relatively distant receptors, while the corresponding evidence for functional preference is weaker and depends on the assay, receptor and experimental context. Structural compatibility is therefore an informative constraint on signalling, not a substitute for measuring signalling itself.

The archive is not functionally arbitrary. In the available onset-kinetic panel, the captured family was usually the most rapidly activated, suggesting that structural sampling frequently follows prominent coupling routes. Yet the mismatches are instructive. Some Gs-containing structures had no detectable Gs response in that kinetic assay, even though several of the same receptors showed Gs coupling with other readouts. This is not necessarily a contradiction: biosensor design, expression levels, subtype coverage, ligand conditions and experimental stabilisation alter what each platform reports. The deposited complex records one accessible or experimentally favoured state, whereas measured signalling includes kinetic and cellular constraints that may differ across assays. Structural capture and functional activation should therefore be compared, not conflated.

The models sharpen that boundary. Structural scores discriminated activation by partners absent from the deposited complex only modestly in one kinetic dataset; changing the Gq-family definition weakened that association, and the available independent assays did not reproduce it. A simple sequence comparator could match or exceed the structural score under some tests, and the most stringent evolutionary comparisons contained too few independent receptor groups for a stable conclusion. These qualifications do not undermine the captured-partner result. Rather, they identify the much stronger claim that the study cannot support: that a geometry learned from mature complexes yields a general predictor of signalling kinetics, coupling strength or pathway preference across assay conditions.

The structural comparisons explain part of the difficulty. Across receptors, characteristic differences in TM6 opening and intracellular cavity shape accompany different captured G-protein families. Much of that contrast faded when the same receptor was compared with itself, and matched α5-helix analyses found no class-wide direction of displacement. The simplest interpretation is not that the interface contains no selectivity information, but that this information is implemented in different structural contexts across receptors. Earlier experiments and structural studies have described receptor-specific solutions involving common G-protein positions and distinct local interactions[9,18–20]. The broad census reveals why an apparently consistent archive-wide feature need not represent a movement used by every individual receptor.

The small 5-HT$_1$A ligand series adds a complementary caution. Ligands that make different local contacts can be associated with related receptor–Gα contact patterns in selected mature complexes. With so few structures, dependent comparisons and a limited range of verified functional responses, this is not evidence that ligand chemistry becomes irrelevant once a G protein binds. It illustrates a narrower point: a stable endpoint can preserve less obvious information about the route taken to reach it than the preceding molecular events may contain.

What, then, would allow us to observe signalling selection rather than infer it from its endpoint? A GPCR must encounter a G protein, form early contacts, promote GDP release, pass through nucleotide-dependent intermediates and ultimately release an activated partner. Different partners may traverse these steps at different rates or with different probabilities even if their mature interfaces are structurally compatible. Time-resolved work on selected GPCR systems demonstrates that such stages can involve distinct conformations and pathways[20–24]. The current archive does not measure the populations or rate constants of those intermediates, so it cannot identify the moment of selection or show that intermediates cause the observed gap between geometry and function. But it offers a clear reason to test that possibility.

The next experiments should therefore compare competing partners under matched conditions, rather than resolve one additional endpoint at a time. For receptors known to activate more than one G-protein family, time-resolved BRET or FRET, rapid-mixing nucleotide-exchange measurements and, where feasible, single-molecule or time-resolved structural methods could quantify partner recruitment, formation of nucleotide-free complexes, GDP release and GTP-dependent dissociation with the same ligand and receptor preparation. Measurements of receptor and transducer expression, ligand occupancy and assay detection limits would be essential. If the earliest partner-specific rate differences arise before the mature interface forms, those kinetics should explain preferences that endpoint geometry misses. If mature-state features predict relative activation after these conditions are controlled, the endpoint description would have greater explanatory reach than the present comparisons suggest.

Computation can make this test more discriminating. Molecular simulations initiated from the measured encounter, GDP-bound and nucleotide-free states could map alternative coupling pathways, while

enhanced sampling and validated kinetic models could estimate transition probabilities and rates rather than merely compare final conformations. State-resolved experimental observables would be needed to constrain the ensembles and test the proposed pathways; a simulated intermediate is not itself proof of productive signalling. Such approaches should also examine membrane composition, ligand state and partner concentration, which may influence access to the same mature structure. The limiting factor is not simply the number of static structures, but the absence of shared kinetic and state-resolved benchmarks against which their biological meaning can be judged.

Several boundaries remain. The archive is shaped by which receptors have been solved and by their ligands, constructs, stabilisers and structural resolution. The broad kinetic comparison comes from a single experimental platform, alternative assays do not measure identical endpoints, and measured zeros and missing reports cannot be treated interchangeably. Some evolutionary tests are dominated by large sequence clusters; the same-receptor and ligand analyses are necessarily sparse. The present work neither shows that all selectivity is kinetic nor rules out receptor-specific determinants visible in a static structure. It establishes a more useful starting point: mature GPCR–G protein structures identify arrangements that can be captured, whereas the preference for one signalling route over another remains a question about the process of activation. Answering it will require structural detail to be connected to time, rather than interpreted in isolation.

Methods

Structural census and annotation

Experimental class A entries were assembled from the Protein Data Bank and harmonised with GPCRdb and GproteinDb annotations[26,27]. Receptor residues were mapped to generic positions using the GPCRdb scheme[30] and coordinates processed with Biotite[31]. Activation labels were taken directly from the harmonised GPCRdb structural-state annotation, with ambiguous entries excluded and no label inferred from the geometric measurements used by the classifier. Because that assignment itself draws on intracellular criteria, the activation analysis is a structural-state positive control rather than independent biochemical validation. Captured-class analyses reduced repeated structures to 207 receptor–transducer units from 169 receptor entries under predefined quality and representativeness

rules. A receptor–transducer structural unit is one curated receptor pairing with the class-defining transducer present in a deposited experimental complex, including engineered mini-G proteins or peptide mimetics when these identify a captured class. It is not an independent experimental specimen. Grouped validation treated receptor orthologues as separate entries; sequence-identity-cluster validation kept closely related orthologues in the same cluster. Census construction, label granularity and functional-repertoire audit tables are provided in Supplementary Tables 1–2, 14, 19, 21, 26 and 30.

Specimen-level provenance audit

Candidate receptor-only references were first defined at the coordinate level from mmCIF polymer entities, under a ligand-permissive definition allowing extracellular peptide or protein ligands but excluding G proteins, arrestins, GRKs, intracellular binders, fusions and unresolved additional proteins, and under a strict definition requiring the receptor to be the sole polymer entity. Because receptor-only coordinates can be produced by focused or local refinement of particles from transducer-containing specimens, coordinate-level candidates were then audited at the specimen level using the deposited entry title, the electron-microscopy sample description, EMDB and PDB relationships, particle counts and the primary publication. A reference was classified as experimentally partner-free only when its specimen contained no intracellular transducer or stabilising partner and its primary publication did not describe the receptor as inactive. Coordinate-only reference controls, construct audits and specimen-provenance exclusions are detailed in Supplementary Tables 7–8, 10, 13, 20 and 22–25.

Structural descriptors and predictive models

Receptor-side geometric measurements comprise conserved microswitch distances and orientations, transmembrane and intracellular-loop descriptors (including ICL2), and intracellular cavity measures. The full descriptor representation contained 107 transformed inputs, including two derived from functional annotation, an activation-consensus score and its completeness count, and 11 acquisition-context inputs. The activation-consensus variables were absent from the independent per-structure

measurement table used for clean refitting, leaving 105 reimplemented inputs before additional exclusions. From that set, the Source Data 18 coordinate-only model removes acquisition variables; its strict-coordinate variant also removes three completeness indicators, yielding macro ROC AUC 0.775, 0.737, 0.678 and 0.493 across the four validation schemes. Source Data 24 separately rebuilds 89 numeric coordinate features and amino acid identities at 64 conserved generic positions. Primary captured-class comparisons in Fig. 3 use this clean 89-feature refit; predictions from the 107-input representation are reported only as explicitly identified sensitivity analyses. At 50% identity, the 107-input coordinate model gives a ROC AUC of 0.731 and the strict-coordinate refit 0.737. Distances are reported in Å, angles in degrees, and missing coordinates were imputed only within training folds. Receptor-side measurements excluded all bound G protein atoms. Four activation-state features comprise the TM3 3.50–TM6 6.34 distance, TM3–TM7 distance, PIF 5.50–6.44 distance and Y7.53 displacement. The within-receptor coordinate-level comparison additionally used 92 numeric descriptors measured on both receptor-only and bound endpoints. Multiclass elastic-net logistic regression was used for the original archive-wide analysis and nested L2 logistic regression for evolutionary-transfer comparisons. Structural-state benchmarks, descriptor extensions, within-receptor tests and model controls are documented in Supplementary Tables 3–6, 9, 11–12, 17–18, 27–29 and 31–34.

Comparison with measured G protein activation kinetics

Published rates were taken from Masuho et al.[14], Supplementary Table S1 (mmc2.xlsx), for 124 receptors. Seventy-seven receptors (94 structural units) overlap the current structural census. I used the first reported receptor isoform where multiple rows occurred (HTR7A rather than HTR7B), following the original analysis, and parsed GαoA, Gαq and Gαs numerical onset rates as the primary Gi/o, Gq/11 and Gs family representatives. All 127 nonempty source rows had numeric values (including zero) in the four assayed columns used here; no blank or nonnumeric value was silently converted into a measured zero. An alternative family-level definition uses max(Gαq,Gα15) and was used for the phylogenetic analysis (see Phylogenetic distribution of transducer preference). That definition changes 34 Gq/11 outcomes among the 188 uncaptured pairs in the full 77-receptor cohort and reduces the primary AUC from 0.705 to 0.620. Neither definition is a universal truth about Gq/11 coupling: Gα15

can be promiscuous and is not interchangeable with Gαq for a subtype-specific kinetic statement. Source Data 27 provides receptor-level labels, per-family positive and negative counts, cluster-bootstrap intervals and reproducible code for both definitions. A rate greater than zero denotes detectable response in the published assay, not general biological coupling. The probabilities tested are frozen out-of-fold predictions trained on captured structural class, not on experimental kinetic outcomes. Kinetic-rank baselines, alternative detection definitions, external assays and evolutionary-locality sensitivity tests are detailed in Supplementary Tables 35–44 and 46–47.

The Avet ebBRET[12] and Inoue Gα-shedding[10] panels were retained as separate external functional resources using the Hauser common-coupling-map[13] tables. To avoid treating unreported observations as experimentally negative, I describe these outcomes as presence of a reported response, not absence of activation. Clean structural scores were evaluated retrospectively on overlapping receptors (53 units/44 receptors for ebBRET and 83 units/67 receptors for shedding); the resulting AUCs are not direct replication tests of Masuho's measured-zero kinetic endpoint. Receptor-clustered bootstrap intervals used 2,000 resamples; the scripts and output tables are included in Source Data 26. Alternative published receptor surface-expression measurements were obtained from Tedman et al.[32] (using processed canonical GPCR entries in the Howard repository), matched to 75 cohort receptors by gene symbol and analysed only as an exploratory context sensitivity (Source Data 27). These expression values come from a different cellular assay and do not permit correction of Masuho-specific receptor-expression effects.

Comparison of structural and sequence representations

Frozen out-of-fold values and fold assignments from the primary models were retained for sensitivity analyses, while the Source Data 24 refit separately models the captured-class target using 89 numeric receptor-coordinate measurements and amino acid identity at 64 conserved generic positions. All refitted models used nested L2 logistic regression with the regularisation strength tuned on eleven logarithmically spaced values by grouped inner cross-validation using negative log loss; numeric imputation and standardisation and categorical imputation and one-hot encoding were fitted only inside each training fold. Outer fold assignments were held fixed. The primary sequence model tuned regularisation with receptor-grouped inner folds, whereas the independent refit groups inner folds by

the same sequence-identity clusters as the outer fold. Matching that receptor-grouped nesting reproduces the primary sequence AUC within 0.003; the stricter nesting reduces the sequence baseline at intermediate separation and is reported as a distinct analysis. Receptor-clustered bootstrap intervals for independent-refit paired geometry-minus-sequence and combined-minus-sequence AUCs use 2,000 resamples on identical held-out observations (Source Data 24, Supplementary Table 34). The corresponding strict-coordinate differences paired against the primary sequence baseline are arithmetic point comparisons only; no confidence interval was computed for that exact pair of frozen models. These comparisons were specified after the original analyses and are reported as post hoc. For post hoc robustness assessment, matched out-of-fold predictions from each of the three clean refit models were exported without altering their training or outer-fold assignments. Macro ROC AUC and paired geometry-minus-sequence AUC differences were recalculated from the exported predictions with separate code on the 207 aligned units. Three thousand bootstrap resamples selected entire sequence-identity clusters, with within-cluster units retained together; resamples without all three captured classes in each one-versus-rest comparison were excluded. Fixed-prediction leave-one-cluster-out and per-outer-fold comparisons were also computed (Source Data 28). These intervals quantify variation across observed clusters conditional on the fitted predictions, and do not include the effects of independently retraining the nested models. Complementary sequence representations and cluster-level uncertainty controls are reported in Supplementary Tables 15–16 and 45.

Gα pose in the receptor frame

For every pair of complexes of the same receptor with different captured classes, the two receptors were superposed on Cα atoms at conserved transmembrane generic positions x.46, x.50 and x.54 for helices 1 to 7, requiring at least twelve shared anchors, and the resulting transform was applied to the Gα chain. Gα residues were mapped to a common reference numbering by global alignment to human Gαs, and the α5 helix was taken as reference positions 360 to 394 with the inserted C-terminal portion defined as 375 to 394. In the common receptor frame the α5 centroid displacement, terminal residue displacement and axis angle were recorded, together with the receptor transmembrane core RMSD as the receptor-side control. Directional consistency was assessed as the mean pairwise cosine similarity between the normalised α5 centroid displacement vectors of different receptors for the same ordered class pair,

against a null of 2,000 permutations in which the sign of each receptor's vector was flipped at random. Stabilising fragments and engineered Gα constructs were parsed from the mmCIF entity descriptions and recorded for stratification.

Exploratory ligand-contact case study

As a targeted, post hoc biological case study, I reanalysed 15 deposited mmCIF models representing four receptor systems (5-HT_1A, D_1 dopamine, α_2A-adrenergic and melanocortin-1 receptors)[33–36] and the five-structure 5-HT_1A–Gi_1 series from Warren et al.[29]. The receptor-side residue contact set was defined by any receptor heavy atom within 4.5 Å of the resolved orthosteric ligand heavy atoms or of the resolved Gα chain; residue-set overlap was quantified by the Jaccard index $|A \cap B|/|A \cup B|$. The 5-HT_1A ligand components were YFW (8FY8), 7LD (8FYT), YGH (8FYE), YG7 (8FYL) and YLX (8FYX). Gα α5-tip displacement was measured after superposition of receptor Cα positions at generic-numbered core positions, with an alternative broader core alignment as sensitivity analysis. Contact thresholds of 4.0 and 5.0 Å were also tested. Dominant-negative $G\alpha i_1$-containing structures (8FY8, 8FYX) were not pooled with other construct annotations in the matched-construct comparison. Published Gi_1 BRET Emax values were used as reported, without inferring missing numerical values for LSD or 5-MeO-DMT. The five structures yield ten pairwise distances but only five structural observations; no regression, p-value or population-level equivalence inference was attempted. The original publications established ligand-recognition mechanisms[29,33–36]; this analysis solely quantifies the variation of deposited endpoint contact sets. Source Data 29 contains the coordinate files, chains/components, input hashes, executable scripts, and all results.

Phylogenetic distribution of transducer preference

Receptors were represented by the majority residue at each of 64 GPCRdb generic positions carried in the structural metadata, retained when at least 80% of positions were present, and intersected with the activation profiles to give 69 receptors. Pairwise identity was computed over jointly present positions and a neighbour-joining tree[37] built from the complementary distances, midpoint rooted, with negative branch lengths set to zero. Pagel's λ[38] was estimated by maximum likelihood on the resulting variance-covariance matrix with a likelihood-ratio test against $\lambda = 0$, and Blomberg's K[39] was compared with 1,000 tip permutations, both on $\log_{10}$ activation rate per family (Gq/11 taken as the faster of Gαq and

Gα15) with zeros replaced by half the smallest positive rate. The preferred family was analysed by Fitch parsimony[40] against 1,000 tip-label permutations. Agreement in preferred family was binned by pairwise identity with receptor-clustered bootstrap intervals. Identities over conserved generic positions run higher than full-sequence identities, so these bins are not on the scale of the sequence-identity clustering used elsewhere. The analysis plan was fixed and archived before any result was computed and is supplied with Source Data 22. The plan specified Gαq alone for Gq/11; the executed analysis used the faster of Gαq and Gα15, a departure that was not recorded when the analysis was run and is disclosed here.

Statistics

Captured-class discrimination was evaluated by macro ROC AUC on matched held-out structural units under receptor-grouped and sequence-identity-clustered splits. All preprocessing and regularisation choices for the 89-feature refit were fitted within training folds, and 2,000 receptor-clustered bootstrap resamples generated paired geometry-versus-sequence intervals. The independent refit's sequence features are 64 generic-position amino acid identities; a broader full-sequence baseline is not interchangeable with it. Functional ROC analyses use measured-positive non-captured family labels, with receptor-clustered confidence intervals and conditional complete-score-vector permutations within captured class and outer fold (Source Data 25 and 26). Source Data 27 evaluates both Gαq-only and Gαq-or-Gα15 labels and a separate sequence-identity nearest-neighbour baseline on 63 matched receptors with corresponding identity values. Nearest-neighbour kinetics are drawn only from other receptors outside the held-out fold; unlike the captured-class structural classifier, that baseline is supervised directly on experimental rates and is therefore not a strictly like-for-like training comparison. One-neighbour, fixed five-neighbour and alternative identity weightings are reported without choosing a best model post hoc. The matched-pair AUC difference is bootstrapped by receptor, not by individual receptor–family pair. Expression-sensitivity tests are exploratory, and the two-fold 30% stratum is not used to infer a universal threshold. P values from 2,000 permutations have a minimum attainable value of 1/2001; post hoc comparisons are interpreted with attention to multiple testing. The additional 3,000-draw sequence-cluster bootstrap gives 95% paired-difference intervals of +0.038 to +0.200 for 48 identity clusters at 50%, and +0.042 to +0.176 for 20 clusters at 40%; at 30%,

five highly imbalanced clusters make the resulting interval unstable (Source Data 28). These exploratory intervals supplement, rather than replace, the 2,000-draw receptor-clustered intervals used in Fig. 3b.

Use of generative AI tools

OpenAI ChatGPT and Anthropic Claude were used as assistive tools for wording, language polishing and editorial refinement of the manuscript, code review, selected analysis and plotting workflows, and consistency checks between text and exported source tables. The author independently reviewed and verified all code, analyses, numerical results, citations, scientific interpretations and final text. No scientific data were generated by generative artificial intelligence.

Data availability

Coordinates were obtained from the Protein Data Bank and annotated using GPCRdb and GproteinDb. Analysis outputs, code and versioned source materials are associated with GPCR SelectivityMap, version 0.6.0 (version-specific DOI: https://doi.org/10.5281/zenodo.23978504; software concept DOI: https://doi.org/10.5281/zenodo.21820928). Source Data 1–29 accompany this manuscript. In particular, Source Data 25 provides frozen annotation-free structural predictions and kinetic matching; Source Data 26 provides conditional controls and external-assay bootstrap outputs; Source Data 27 includes family-label sensitivity, sequence-neighbour comparison, expression controls and a workbook-independent AUC reproduction; Source Data 28 contains clean-refit held-out predictions and cluster-aware sensitivity scripts; and Source Data 29 contains the exploratory ligand-case inputs, coordinates, provenance and analyses. The Masuho publisher workbook is not redistributed, and external pharmacology and expression datasets retain attribution to their primary sources.

Code availability

GPCR SelectivityMap, version 0.6.0, is available at https://github.com/hbatebi/GPCR-SelectivityMap and is linked to the version-specific Zenodo DOI https://doi.org/10.5281/zenodo.23978504 (concept DOI: https://doi.org/10.5281/zenodo.21820928). Analyses used Python, including NumPy, pandas, SciPy, scikit-learn, Biopython, Matplotlib and Biotite; the ligand-contact case study additionally used gemmi. Additional analysis scripts and outputs are supplied in Source Data 25–29. The Source Data 27

AUC reproducer operates on archived per-receptor labels without redistributing the original Masuho supplementary workbook. Source Data 28 reproduces fixed-prediction cluster-aware sensitivity analyses; it does not regenerate geometric descriptors from raw PDB coordinates. The ligand-case workflow and input records are supplied with Source Data 29.

References

1. Sriram, K. & Insel, P. A. G protein-coupled receptors as targets for approved drugs: how many targets and how many drugs? Mol. Pharmacol. 93, 251–258 (2018).
2. Hauser, A. S., Attwood, M. M., Rask-Andersen, M., Schiöth, H. B. & Gloriam, D. E. Trends in GPCR drug discovery: new agents, targets and indications. Nat. Rev. Drug Discov. 16, 829–842 (2017).
3. Alexander, S. P. H. et al. The Concise Guide to PHARMACOLOGY 2025/26: G protein-coupled receptors. Br. J. Pharmacol. 182 (S1), S24–S151 (2025).
4. Kenakin, T. & Christopoulos, A. Signalling bias in new drug discovery: detection, quantification and therapeutic impact. Nat. Rev. Drug Discov. 12, 205–216 (2013).
5. Smith, J. S., Lefkowitz, R. J. & Rajagopal, S. Biased signalling: from simple switches to allosteric microprocessors. Nat. Rev. Drug Discov. 17, 243–260 (2018).
6. Shoichet, B. K. & Kobilka, B. K. Structure-based drug screening for G-protein-coupled receptors. Trends Pharmacol. Sci. 33, 268–272 (2012).
7. Congreve, M., de Graaf, C., Swain, N. A. & Tate, C. G. Impact of GPCR structures on drug discovery. Cell 181, 81–91 (2020).
8. Jumper, J. et al. Highly accurate protein structure prediction with AlphaFold. Nature 596, 583–589 (2021).
9. Flock, T. et al. Selectivity determinants of GPCR–G-protein binding. Nature 545, 317–322 (2017).
10. Inoue, A. et al. Illuminating G-protein-coupling selectivity of GPCRs. Cell 177, 1933–1947.e25 (2019).
11. Okashah, N. et al. Variable G protein determinants of GPCR coupling selectivity. Proc. Natl. Acad. Sci. U. S. A. 116, 12054–12059 (2019).
12. Avet, C. et al. Effector membrane translocation biosensors reveal G protein and β-arrestin coupling profiles of 100 therapeutically relevant GPCRs. eLife 11, e74101 (2022).
13. Hauser, A. S. et al. Common coupling map advances GPCR–G protein selectivity. eLife 11, e74107 (2022).
14. Masuho, I. et al. Rules and mechanisms governing G protein coupling selectivity of GPCRs. Cell Rep. 42, 113173 (2023).
15. Matic, M., Miglionico, P., Tatsumi, M., Inoue, A. & Raimondi, F. GPCRome-wide analysis of G-protein-coupling diversity using a computational biology approach. Nat. Commun. 14, 4361 (2023).
16. Huang, S. et al. GPCRs steer Gi and Gs selectivity via TM5–TM6 switches as revealed by structures of serotonin receptors. Mol. Cell 82, 2681–2695.e6 (2022).
17. Sandhu, M. et al. Dynamic spatiotemporal determinants modulate GPCR:G protein coupling selectivity and promiscuity. Nat. Commun. 13, 7428 (2022).
18. Mobbs, J. I. et al. Structures of the human cholecystokinin 1 (CCK1) receptor bound to Gs and Gq mimetic proteins provide insight into mechanisms of G protein selectivity. PLoS Biol. 19, e3001295 (2021).
19. Alegre, K. O. et al. Structural basis and mechanism of activation of two different families of G proteins by the same GPCR. Nat. Struct. Mol. Biol. 28, 936–944 (2021).
20. Kobayashi, K. et al. The dynamic basis of G-protein recognition and activation by a GPCR. Nature 652, 812–821 (2026).
21. Papasergi-Scott, M. M. et al. Time-resolved cryo-EM of G-protein activation by a GPCR. Nature 629, 1182–1191 (2024).
22. Batebi, H. et al. Mechanistic insights into G-protein coupling with an agonist-bound G-protein-coupled receptor. Nat. Struct. Mol. Biol. 31, 1692–1701 (2024).
23. Khan, S. et al. Structural snapshots capture nucleotide release at the μ-opioid receptor. Nature 648, 755–763 (2025).
24. Robertson, M. J. et al. Non-equilibrium snapshots of ligand efficacy at the μ-opioid receptor. Nature 652, 794–802 (2026).
25. Wallach, I. & Heifets, A. Most ligand-based classification benchmarks reward memorization rather than generalization. J. Chem. Inf. Model. 58, 916–932 (2018).
26. Pándy-Szekeres, G. et al. GPCRdb in 2023: state-specific structure models using AlphaFold2 and new ligand resources. Nucleic Acids Res. 51, D395–D402 (2023).
27. Pándy-Szekeres, G. et al. GproteinDb in 2024: new G protein–GPCR couplings, AlphaFold2-multimer models and interface interactions. Nucleic Acids Res. 52, D466–D475 (2024).

28. Janicot, R. et al. Direct interrogation of context-dependent GPCR activity with a universal biosensor platform. Cell 187, 1527–1546.e25 (2024).
29. Warren, A. L. et al. Structural pharmacology and therapeutic potential of 5-methoxytryptamines. Nature 630, 237–246 (2024).
30. Isberg, V. et al. Generic GPCR residue numbers: aligning topology maps while minding the gaps. Trends Pharmacol. Sci. 36, 22–31 (2015).
31. Kunzmann, P. & Hamacher, K. Biotite: a unifying open source computational biology framework in Python. BMC Bioinformatics 19, 346 (2018).
32. Tedman, A. et al. Efficient experimental characterization of the GPCRome via deep receptor scanning. Nat. Commun. https://doi.org/10.1038/s41467-026-76564-7 (2026).
33. Xu, P. et al. Structural insights into the lipid and ligand regulation of serotonin receptors. Nature 592, 469–473 (2021).
34. Teng, X. et al. Ligand recognition and biased agonism of the D1 dopamine receptor. Nat. Commun. 13, 3186 (2022).
35. Lou, J. S. et al. Distinct binding conformations of epinephrine with alpha- and beta-adrenergic receptors. Exp. Mol. Med. 56, 1952–1966 (2024).
36. Ma, S. et al. Structural mechanism of calcium-mediated hormone recognition and Gβ interaction by the human melanocortin-1 receptor. Cell Res. 31, 1061–1071 (2021).
37. Saitou, N. & Nei, M. The neighbor-joining method: a new method for reconstructing phylogenetic trees. Mol. Biol. Evol. 4, 406–425 (1987).
38. Pagel, M. Inferring the historical patterns of biological evolution. Nature 401, 877–884 (1999).
39. Blomberg, S. P., Garland, T. Jr & Ives, A. R. Testing for phylogenetic signal in comparative data: behavioral traits are more labile. Evolution 57, 717–745 (2003).
40. Fitch, W. M. Toward defining the course of evolution: minimum change for a specific tree topology. Syst. Zool. 20, 406–416 (1971).

Acknowledgements

This work used publicly deposited coordinates from the Protein Data Bank, receptor annotations and generic residue numbering from GPCRdb and GproteinDb, and the published G protein activation kinetics of Masuho and co-workers. The author thanks the depositors and curators of those resources.

Author contributions

H.B. is the sole author, and conceived the study, performed all analyses, prepared all figures and wrote the manuscript.

Competing interests

The author declares no competing interests.

Figure legends

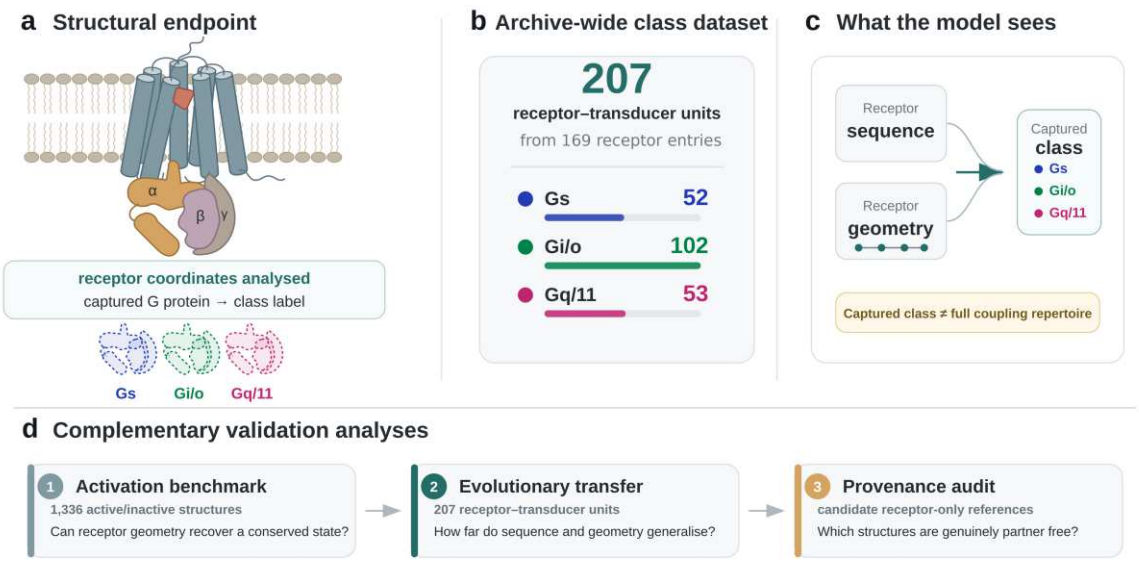


Fig. 1 | What can GPCR structures tell us about G-protein selectivity? (a) A representative mature GPCR–G protein complex: the captured transducer defines the deposited structural partner, not a measured signalling preference. (b) The curated receptor–transducer units by captured G-protein family, drawn from 169 receptor entries (164 nonredundant receptor identities). (c) Receptor sequence and geometry extracted from mature complexes are used in the computational comparisons. (d) Complementary tests of structural activation state, transfer across receptor families and experimental provenance. A structural unit is one curated receptor–transducer pairing, not one independent biological specimen.

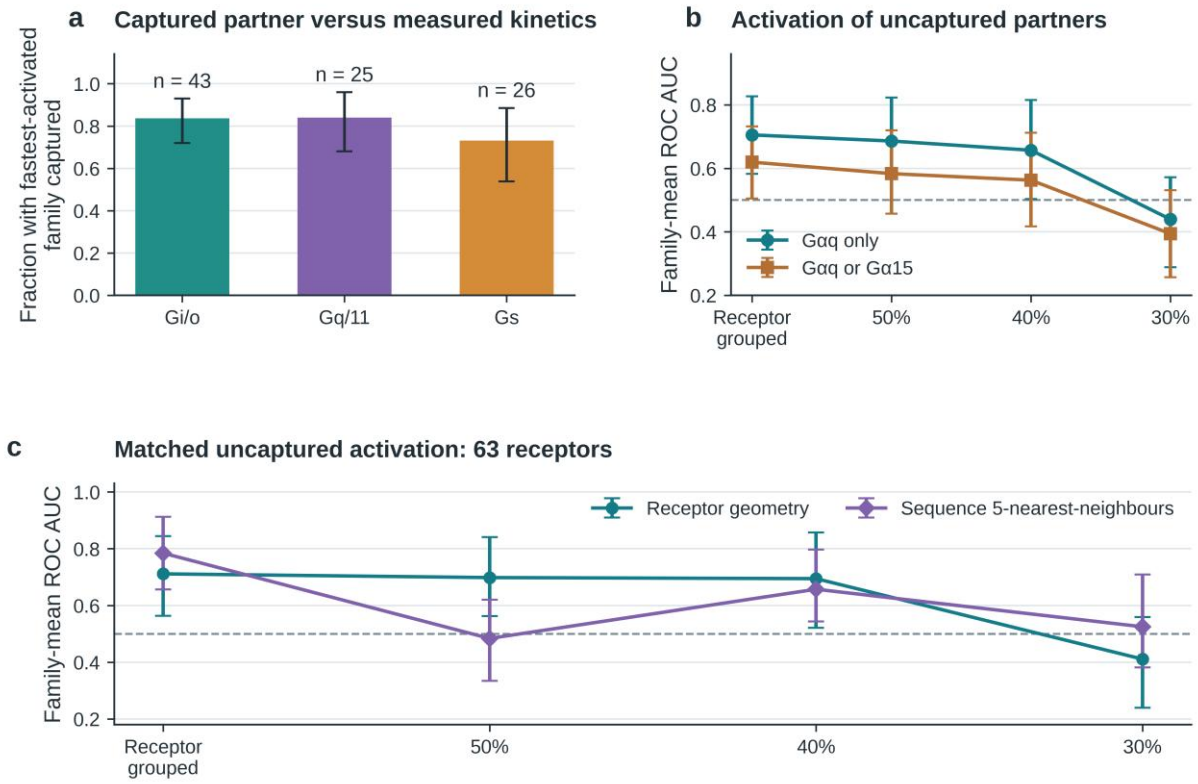


Fig. 2 | Captured G proteins frequently match kinetic preference. (a) Agreement between the G-protein family present in a structure and the family activated most rapidly in published onset-kinetic measurements (94 structural units from 77 receptors). (b) Ability of receptor-geometry scores to distinguish detectable responses for uncaptured G-protein families, comparing the primary Gαq definition with one that also counts Gα15 (188 observations; 95% receptor-clustered confidence intervals). (c) Comparison with a sequence-neighbour benchmark trained on measured functional labels in the overlapping receptors. Panels b and c classify detectable activation, not absolute activation rates. These panels address different prediction tasks and training targets. Confidence intervals are clustered by receptor; the 30% sequence-identity split has limited valid folds. Unreported responses in independent assays are not treated as measured negatives.



Fig. 3 | Receptor geometry identifies captured partners beyond close homologues. (a) Discrimination of the captured G-protein family using conserved sequence positions, receptor-coordinate geometry or both, with receptors or sequence-identity clusters held out. (b) Paired geometry-minus-sequence differences and receptor-clustered confidence intervals for the matched model predictions. (c) A separate analysis within receptors that were solved with multiple partner classes, contrasting the observed class-probability margin with label-permutation controls. The most stringent 30% identity test has only two usable, unequal folds. Cluster-resampled intervals and largest-cluster sensitivity tests are provided in Supplementary Table 45 and Supplementary Fig. 11 (Source Data 28); the confidence intervals shown in panel b are receptor-clustered. Panels a–b use the independently refitted models in Source Data 24; panel c is based on the separate Source Data 18 specification. P values in panel c refer to the class-probability margin; the corresponding within-receptor accuracies are given in Supplementary Table 33.

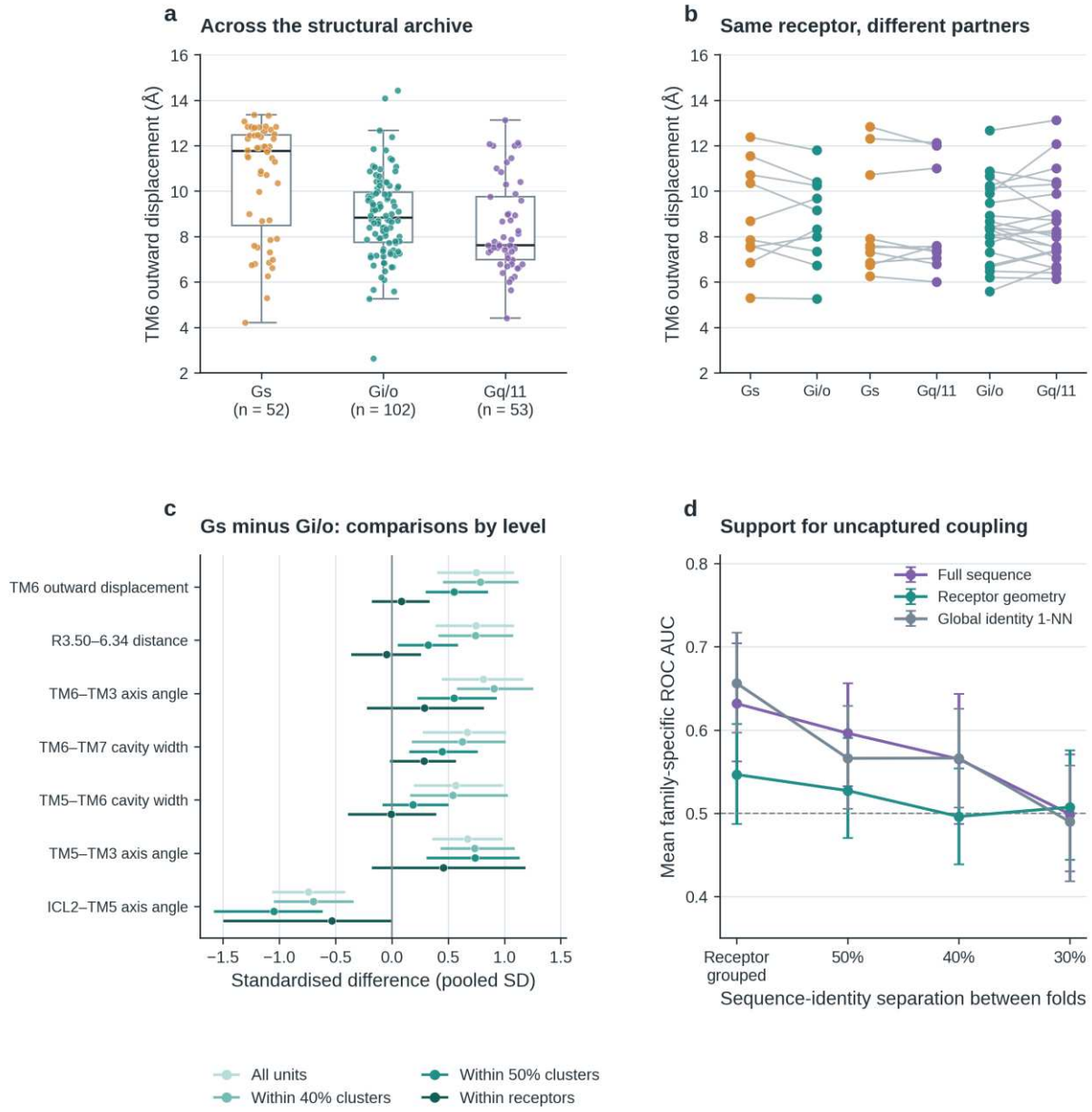


Fig. 4 | Class-associated structural differences weaken within individual receptors. (a) Intracellular displacement of TM6 in structures captured with different G-protein families. (b) Comparisons between partner classes within receptors solved more than once; connected points belong to the same receptor. (c) Class-associated differences in intracellular descriptors across all structures, within sequence-identity clusters and within the same receptor, with confidence intervals. (d) Complementary analysis of additional coupling support in the curated functional map, comparing sequence-based and geometric representations under different validation splits. These panels distinguish archive-wide associations from within-receptor differences rather than identifying causal selectivity determinants.

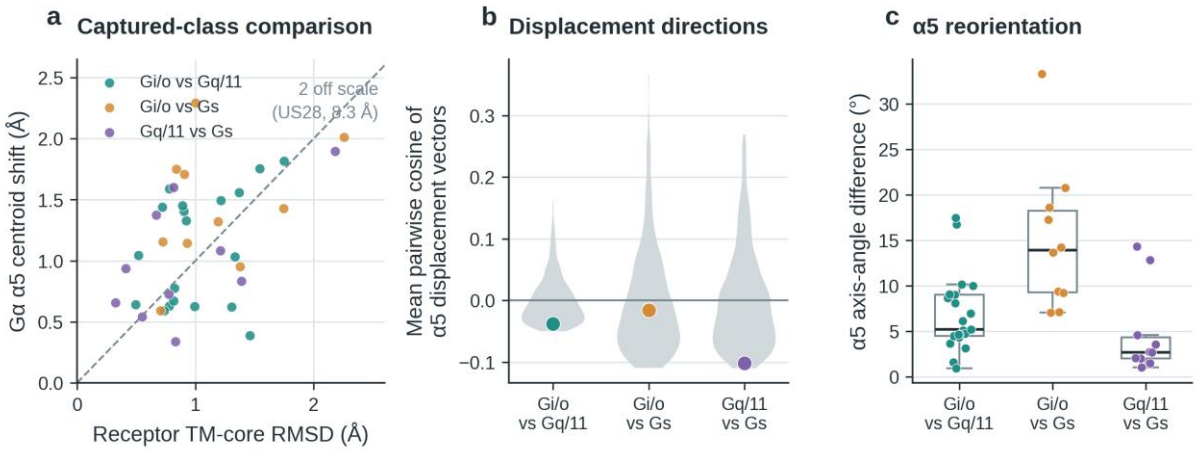


Fig. 5 | G-protein engagement lacks a universal geometric rearrangement. (a) Receptor-core displacement compared with movement of the Gα α5-helix centre across matched complexes of the same receptor (41 comparisons). (b) Similarity in the direction of α5 movement across receptors, compared with sign-flip permutation controls. (c) Difference in α5 orientation for different partner-class pairs. These are comparisons among mature, stabilised structures; they do not describe the path or kinetics of G-protein binding.

Supplementary Files

This is a list of supplementary files associated with this preprint. Click to download.

- BatebiSupplementary.docx
- SourceData129.zip